Table 3. MMR suppression of duplication-mediated GCRs during S and G2/M stages.

Relevant genotype	Strain RDKY	GCR rate* (fold increase)
Wild-type	6678	4.1 [3.1–6.6] × 10^{-8} (1)
*msh6*Δ	6714	2.2 [1.6–2.7] × 10^{-7} (5.3)
G2/M-MSH6	7685	4.0 [2.8–7.4] × 10^{-8} (1.0)
S-MSH6	7686	9.1 [5.7–16.4] × 10^{-8} (2.2)

*Rate of 5FOA^R Can^R progeny. The number in parentheses represents the fold increase relative to the wild-type GCR rate.

pathway (*20*). Furthermore, Msh2-Msh6–dependent MMR is completely dependent on the PCNA coupling of Msh2-Msh6 to replication factories in *exo1* mutants (*20*). Thus, PCNA may provide a physical signal for coupling of one of the MMR pathways to the replication fork, whereas the signal for the second MMR pathway is unknown. Other possibilities for the repair signals are single-stranded gaps and nicks transiently generated by DNA replication (*21*), which is consistent with the requirement for a nick in MMR in vitro (*22*, *23*). The signals triggering MMR on mitotic and meiotic recombination intermediates and for initiating heteroduplex rejection, which differs from MMR due to modified protein requirements (*16*, *24*, *25*), are presently unclear but could be nicks, gaps, branched structures, or the mispairs in the DNA intermediates.

References and Notes

1. B. D. Harfe, S. Jinks-Robertson, *Annu. Rev. Genet.* **34**, 359 (2000).
2. R. R. Iyer, A. Pluciennik, V. Burdett, P. L. Modrich, *Chem. Rev.* **106**, 302 (2006).
3. R. D. Kolodner, G. T. Marsischky, *Curr. Opin. Genet. Dev.* **9**, 89 (1999).
4. G. T. Marsischky, N. Filosi, M. F. Kane, R. Kolodner, *Genes Dev.* **10**, 407 (1996).
5. E. A. Sia, R. J. Kokoska, M. Dominska, P. Greenwell, T. D. Petes, *Mol. Cell. Biol.* **17**, 2851 (1997).
6. C. Chen, B. J. Merrill, P. J. Lau, C. Holm, R. D. Kolodner, *Mol. Cell. Biol.* **19**, 7801 (1999).
7. H. Flores-Rozas, D. Clark, R. D. Kolodner, *Nat. Genet.* **26**, 375 (2000).
8. A. B. Clark, F. Valle, K. Drotschmann, R. K. Gary, T. A. Kunkel, *J. Biol. Chem.* **275**, 36498 (2000).
9. S. S. Shell, C. D. Putnam, R. D. Kolodner, *Mol. Cell* **26**, 565 (2007).
10. J. K. Hood, W. W. Hwang, P. A. Silver, *J. Cell Sci.* **114**, 589 (2001).
11. G. I. Karras, S. Jentsch, *Cell* **141**, 255 (2010).
12. C. Hendrickson, M. A. Meyn 3rd, L. Morabito, S. L. Holloway, *Curr. Biol.* **11**, 1781 (2001).
13. R. Wäsch, F. R. Cross, *Nature* **418**, 556 (2002).
14. M. K. Raghuraman *et al.*, *Science* **294**, 115 (2001).
15. C. Chen, K. Umezu, R. D. Kolodner, *Mol. Cell* **2**, 9 (1998).
16. A. Datta, A. Adjiri, L. New, G. F. Crouse, S. Jinks Robertson, *Mol. Cell. Biol.* **16**, 1085 (1996).
17. I. Matic, C. Rayssiguier, M. Radman, *Cell* **80**, 507 (1995).
18. C. D. Putnam, T. K. Hayes, R. D. Kolodner, *Nature* **460**, 984 (2009).
19. T. L. Orr-Weaver, J. W. Szostak, *Microbiol. Rev.* **49**, 33 (1985).
20. H. Hombauer, C. S. Campbell, C. E. Smith, A. Desai, R. D. Kolodner, *Cell* **147**, 1040 (2011).
21. L. D. Langston, M. O'Donnell, *Mol. Cell* **23**, 155 (2006).
22. Y. Zhang *et al.*, *Cell* **122**, 693 (2005).
23. N. Constantin, L. Dzantiev, F. A. Kadyrov, P. Modrich, *J. Biol. Chem.* **280**, 39752 (2005).
24. N. Sugawara, T. Goldfarb, B. Studamire, E. Alani, J. E. Haber, *Proc. Natl. Acad. Sci. U.S.A.* **101**, 9315 (2004).
25. K. Myung, A. Datta, C. Chen, R. D. Kolodner, *Nat. Genet.* **27**, 113 (2001).

Acknowledgments: This study was supported by NIH grant GM50006 (to R.D.K.).

Supporting Online Material

www.sciencemag.org/cgi/content/full/334/6063/1713/DC1
Materials and Methods
Figs. S1 and S2
Table S1
References (*26*, *27*)

6 July 2011; accepted 31 October 2011
10.1126/science.1210770

Model-Driven Engineering of RNA Devices to Quantitatively Program Gene Expression

James M. Carothers,[1] Jonathan A. Goler,[2] Darmawi Juminaga,[1] Jay D. Keasling[1,2,3]*

The models and simulation tools available to design functionally complex synthetic biological devices are very limited. We formulated a design-driven approach that used mechanistic modeling and kinetic RNA folding simulations to engineer RNA-regulated genetic devices that control gene expression. Ribozyme and metabolite-controlled, aptazyme-regulated expression devices with quantitatively predictable functions were assembled from components characterized in vitro, in vivo, and in silico. The models and design strategy were verified by constructing 28 *Escherichia coli* expression devices that gave excellent quantitative agreement between the predicted and measured gene expression levels (r = 0.94). These technologies were applied to engineer RNA-regulated controls in metabolic pathways. More broadly, we provide a framework for studying RNA functions and illustrate the potential for the use of biochemical and biophysical modeling to develop biological design methods.

Functional complexity that emerges from component interactions is a universal feature of physical systems (*1*). As a consequence, in most engineering disciplines, tools for simulating and designing global functions from local component behaviors are essential for constructing complex devices and systems (*2*). Biological systems exhibit functional complexity across multiple scales, from RNA, DNA, and protein subunit interactions to those among genes, pathways, circuits, and cells (*3*). Creating biological design tools (*2*) applicable to each of these scales will be crucial for increasing the sizes and complexities of the synthetic biological systems engineered for therapeutic applications (*4*) or for drugs, fuels, and materials production (*5*). In nature, RNA structures process cellular information and regulate genetic expression at the levels of transcription, translation, and RNA degradation (*6*). Synthetic aptamers, ribozymes (rbzs), and aptazymes (aptzs) assembled into static or dynamic ligand-responsive regulators can control gene expression in bacteria, yeast, and mammalian cells (*7*, *8*). Given this functional potential, creating methods to rapidly assemble RNA-regulated devices with predictable activities (*9*) should allow engineering of programmable pathway and circuit controllers (*10*) and higher-order information-processing mechanisms (*11*).

We developed design-driven approaches for engineering static, rbz-regulated expression devices (rREDs) and dynamic, ligand-controlled, aptz-regulated expression devices (aREDs) with quantitatively predictable functions (fig. S1). We used a mechanism for control by static rREDs or dynamic aREDs that is reminiscent of control by the naturally occurring *glmS* riboswitch, which regulates genetic expression through cis cleavage of the 5′ untranslated region (UTR) in *glmS* mRNA that decreases transcript half-life and protein abundance (*12*). In our system, rbz- and aptz-regulated RNA cleavage increases transcript half-life and protein expression as a consequence of RppH– degradation of 5′OH-RNA, which is slow compared with RppH+ degradation of 5′PPP-RNA (*13*). A coarse-grained model of 11 effective rate constants was created to simulate global rRED and aRED functions from local component characteristics (Fig. 1A). To ensure engineering tractability, we formulated the genetic control mechanism and coarse-grained model to emphasize measurable and tunable component characteristics (Fig. 1, B and C, and table S1).

The mechanistic model was evaluated with 4×10^4 Monte Carlo distributions of parameter inputs to map design variable space to the rel-

[1]California Institute for Quantitative Biosciences, University of California, Berkeley, Berkeley CA 94720, USA and Joint BioEnergy Institute, Emeryville, CA 95608, USA. [2]Synthetic Biology Engineering Research Center and Department of Bioengineering, University of California, Berkeley, CA 94720, USA. [3]Department of Chemical and Biomolecular Engineering, University of California, Berkeley and Physical Biosciences Division, Lawrence Berkeley National Laboratory, Berkeley, CA 94720, USA.

*To whom correspondence should be addressed. E-mail: keasling@berkeley.edu

ative rates of gene expression (γ_{rel}) produced as device outputs (Fig. 1C). rRED expression was specified relative to that of reference devices without rbzs to normalize for fluctuations because of effects external to the controller (*14*). Global sensitivity analysis (*15*) showed that all of the rRED design variables had significant partial correlation coefficients (PCCs) with γ_{rel} ($P < 0.05$), indicating that device behavior depended on the functional interactions of multiple components (Fig. 1C and table S2). Across the specified intervals, variations in rbz folding (k_{fold},

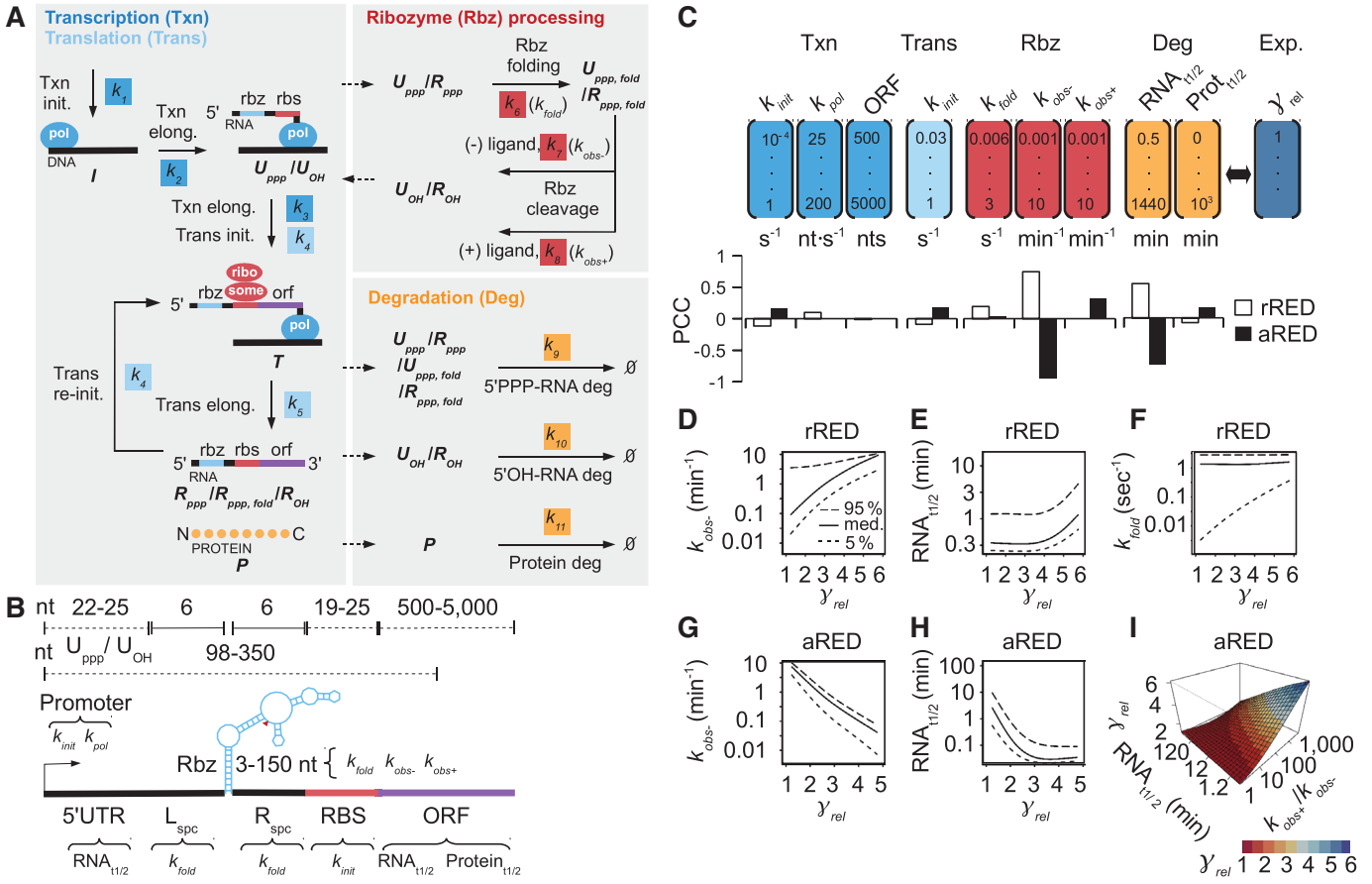

Fig. 1. RNA-regulated expression devices and functional design space. (**A**) Functions of rREDs and aREDs were simulated with a coarse-grained mechanistic model of effective rate constants. (**B**) Tunable components and design variables for static rRED and dynamic aRED genetic controllers. Relationships between the mechanistic model parameters and design variables are detailed in table S1. nt, nucleotides. (**C**) Combinatorial design variable space was mapped to device outputs (γ_{rel}) with Monte Carlo filtering. PCCs with γ_{rel} measure the impact of individual design variables on device behavior. For design variables with the largest PCCs, inputs were filtered by device output and plotted for rREDs (**D** to **F**) and aREDs (**G** and **H**). (**I**) Surface plot of a locally weighted regression of aRED γ_{rel} onto $RNA_{t1/2}$ and ligand-activation ratio (k_{obs+}/k_{obs-}), with residual standard error = 0.14. Also see fig. S3.

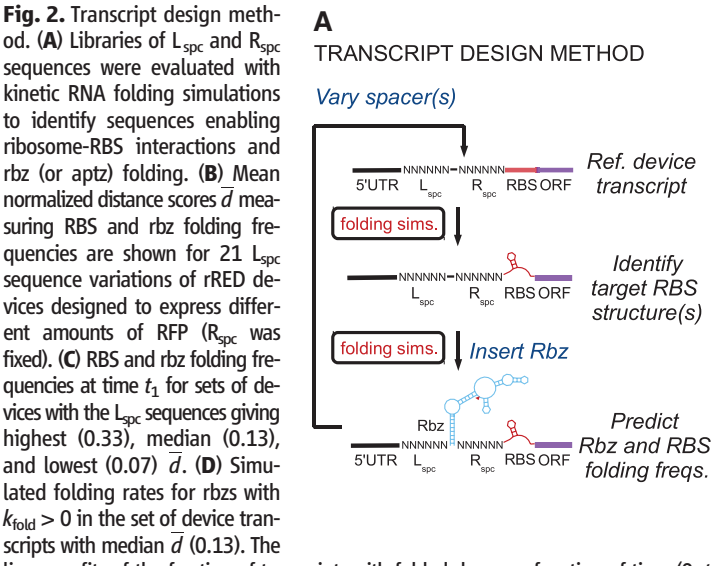

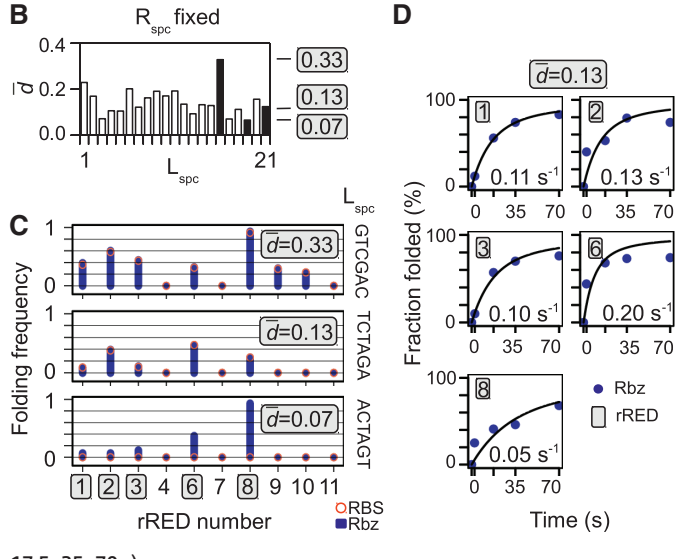

Fig. 2. Transcript design method. (**A**) Libraries of L_{spc} and R_{spc} sequences were evaluated with kinetic RNA folding simulations to identify sequences enabling ribosome-RBS interactions and rbz (or aptz) folding. (**B**) Mean normalized distance scores $\bar{d}$ measuring RBS and rbz folding frequencies are shown for 21 L_{spc} sequence variations of rRED devices designed to express different amounts of RFP (R_{spc} was fixed). (**C**) RBS and rbz folding frequencies at time t_1 for sets of devices with the L_{spc} sequences giving highest (0.33), median (0.13), and lowest (0.07) $\bar{d}$. (**D**) Simulated folding rates for rbzs with $k_{fold} > 0$ in the set of device transcripts with median $\bar{d}$ (0.13). The lines are fits of the fraction of transcripts with folded rbzs as a function of time (0, t_1, 17.5, 35, 70 s).

PCC = 0.17), catalysis (k_{obs-}, 0.66), and RNA half-life ($RNA_{t1/2}$, 0.51) had the largest effects on device function. Filtering the parameter inputs by γ_{rel} identified functional constraints on rRED design variable space, and inspection demonstrated that the magnitude of the response depended on the time scale of rbz folding and cleavage relative to that of the transcript degradation rate (Fig. 1, D to F).

aRED γ_{rel} measured the dynamic range of device outputs generated by saturating ligand concentrations relative to that of a reference state (fig. S2). Minimizing the ligand-free cleavage rate (k_{obs-}) and shortening transcript half-life are expected to reduce reference state expression and increase the dynamic range of aptz-regulated genetic control (*9*). As anticipated, large negative PCCs for k_{obs-} (−0.84) and $RNA_{t1/2}$ (−0.68) and narrow functional parameter ranges (Fig. 1, G and H) indicated that these design variables heavily influence device activities. Consistent with this view, local polynomial regression of the aptz ligand-activation ratio (k_{obs+}/k_{obs-}) and $RNA_{t1/2}$ onto γ_{rel} explained almost 85% of the variation in aRED-programmed expression (Fig. 1I). We obtained 100% increases in ligand-dependent expression, similar to the dynamic ranges generated with aptzs in yeast (*16*), with ligand-activation ratios as small as 20. Thus, although rRED and aRED activities depend on interactions related to multiple component characteristics, our analysis implies that devices meeting a range of targeted performance criteria can be engineered by tuning subsets of the design variables (fig. S3), making the design process simpler than one would have imagined without such a model.

Implementing devices to meet functional specifications requires components with characteristics spanning a range of parameter values. Thus, we generated and characterized 22 different self-cleaving rbzs and aptzs (table S3 and fig. S4). Starting with reported hammerhead rbzs, modifications with semipredictable effects, such as interaction loop point mutations (*17*), were made to modulate tertiary structure folding and tune k_{obs-}, resulting in 12 rbzs with in vitro k_{obs-} values ranging from <0.1 to 3.6 min^{-1}. Seven aptzs responsive to the xanthine alkaloid theophylline (*18*) exhibited in vitro k_{obs-} values as low as 0.01 min^{-1}, k_{obs+} values as high as 0.4 min^{-1}, and ligand-activation ratios (k_{obs+}/k_{obs-}) ranging from 1.5 to 19.3. Also included were 2 *p*-aminophenylalanine (*p*-AF) aptzs that we evolved from an in vitro–selected aptamer (*19*) and the *Schistosoma mansoni* rbz (*18*). Altogether, the set contained self-cleaving RNAs with different lengths, sequences, secondary structure topologies, and catalytic rate constants, and, for the aptzs, various target ligands and ligand-activation ratios.

Because RNA molecules can form stable, misfolded structures, cotranscriptional folding pathways are important determinants of RNA-regulated functions (*20*). We developed a transcript design method to achieve two RNA folding objectives: (i) secondary structures formed with the ribosome binding site (RBS) could not prevent translation initiation (*21*), and (ii) rbz and aptz folding was fast relative to $RNA_{t1/2}$ (Fig. 1). Briefly, the method used kinetic RNA folding simulations (*22*) to screen libraries of spacer sequences (L_{spc} and R_{spc} in Fig. 2A) that enable the RBS and rbz or aptz to fold into target secondary structures in the context of elongating transcripts. Designed transcripts were evaluated by computing a distance score (*d*). For a set of devices engineered to program different amounts of expression, larger values of the mean distance score, $\overline{d}$, normalized on a scale from 0 to 1, signified improved RBS and rbz or aptz folding probabilities.

As an illustration, the mean normalized distance score, $\overline{d}$, was plotted for 21 L_{spc} sequence variants, which were determined from 100 stochastic folding simulations for each of 10 rREDs designed to express various amounts of red fluorescent protein (RFP). The mean distance scores ranged from 0.33 to 0.07 (Fig. 2B), indicating wide variations in predicted folding probabilities at t_1, the approximate time needed for a ribosome to interact with a nascent U_{ppp} transcript RBS (*23*). Compared with the device sets with the lowest ($\overline{d}$ = 0.07, Z = –1.31) and median ($\overline{d}$ = 0.13, Z = –0.36) scores, the highest scoring set ($\overline{d}$ = 0.33, Z = 2.96) had a larger number of rREDs with rbzs predicted to fold (i.e., 7 of 10 rbzs with

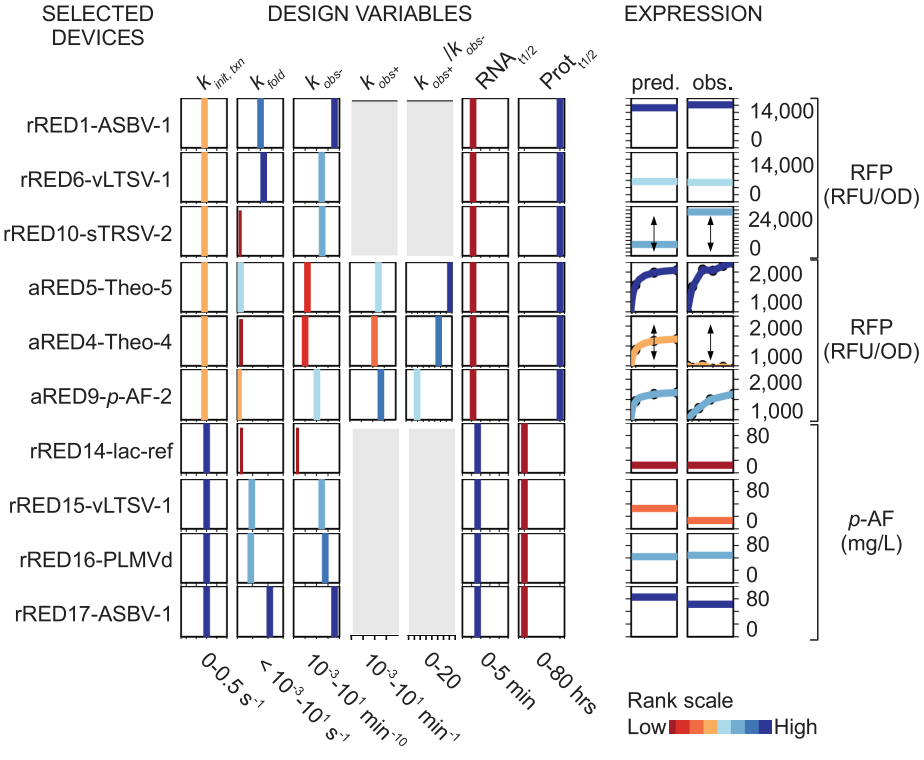

Fig. 3. Programmable rREDs and aREDs. Selected design variables (**left**) and predicted and observed functions (γ_{rel}) (**right**) are graphed. For rREDs and theophylline- and *p*-AF–responsive aREDs expressing RFP, activity is reported in relative fluorescence units [RFU/optical density (OD)]. aRED γ_{rel} predicted corresponds to device outputs with ligand concentrations ([*L*]) defined relative to the EC_{50}, the concentration where aptz cleavage is half maximal ([*L*] = 0, EC_{50}, 5·EC_{50}, 10·EC_{50}, fig. S2). aRED obs. γ_{rel} is plotted as a function of [*L*] (0, 1, 3, 5, 7, 9 mM for theophylline; 0, 0.25, 1, 2.5, 5, 10 mM for *p*-AF). *p*-AF flux produced from the *papABC* operon was programmed with rREDs in the context of an engineered, three-plasmid, 12-gene system (fig. S8). rRED14-lac-ref is a reference device without a rbz. Color indicates rank order. (‡) denotes devices with rbz or aptz k_{fold} < 0; function of those devices is expected to fall outside the domain of the predictive model. See fig. S7 for entire set of 28 engineered devices.

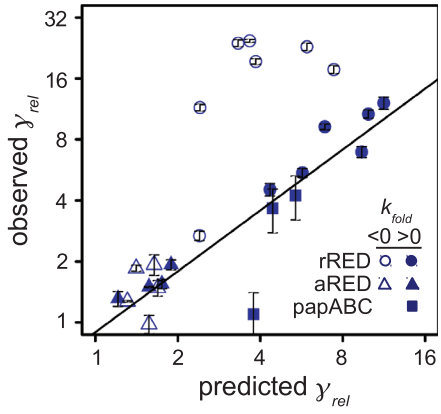

Fig. 4. Predicted and measured device functions. Plot of measured γ_{rel} (observed) versus model-derived, predicted γ_{rel} for 25 engineered rREDs and aREDs (reference devices are not shown). Expression from devices with rbz or aptz k_{fold} > 0 (solid symbols) is expected to fall within the functional domain that can be predicted with the mechanistic model. Line is a fit of data for rREDs and aREDs with rbz or aptz k_{fold} > 0 (solid symbols). Mean ± SD shown.

predicted $k_{fold} > 0$). Although the sets with the lowest and median scores both had 5 rREDs with rbz $k_{fold} > 0$, only the set with median $\overline{d}$ had RBSs predicted to fold into the target structures as defined by the ensemble of RBS folds for reference device transcripts (Fig. 2C).

Extending the cotranscriptional folding simulations beyond t_1 provided data for estimating rbz folding rates. For example, for rREDs from the set with median $\overline{d}$, large fractions of the rbzs with $k_{fold} > 0$ at t_1 (rREDs 1, 2, 3, 6, and 8) were predicted to fold into the target structures during the lifetime of the RFP mRNA. RBS folding was highly correlated with rbz folding within these devices (Pearson's $r = 0.99$), and the predicted rbz folding rates ranged from 0.05 to 0.20 s^{-1} (Fig. 2D). Thus, although any given combination of spacer sequences may be suboptimal for a particular device, motifs identified through sparse library searches may enable RBS and rbz or aptz folding and the construction of devices with targeted functions (fig. S5 and table S4).

To demonstrate that variations in tunable design parameters generate quantitatively predictable outputs, we constructed 24 genetic devices to program amounts of RFP. For each rRED and aRED, predicted γ_{rel} was modeled with component characteristics obtained in vitro, in vivo, in silico, and from reported values and compared to RFP production measured in vivo (table S6 and fig. S7). Results for selected devices highlighted several aspects of the engineering strategy (Fig. 3). For instance, rRED1 was designed to produce the highest amount of protein in the set, and the predicted and observed abundances of RFP were in very good quantitative agreement [pred. = 11,300 ± 400, obs. = 12,100 ± 800 relative fluorescence units (RFU)]. In accordance with the design parameters, rRED6 produced 50% less RFP than rRED1 because rRED6 k_{obs-} (0.3 min^{-1}) was one-tenth that of rRED1 k_{obs-} (3.6 min^{-1}). Similarly, the measured results closely matched the predicted dynamic ranges for aREDs responsive to theophylline (aRED5) and *p*-AF (aRED9) even though the in vitro aptz ligand-activation ratios and specified amounts of expression were very different. In contrast, although the design parameters for rRED6 and rRED10 were nearly identical, the predicted rRED10 rbz k_{fold} was <0, and sharply different expression outputs were generated as a result. Likewise, despite a large aptz ligand-activation ratio, aRED4, with aptz $k_{fold} < 0$, produced no ligand-dependent RFP expression in the cell. Consistent with expectation, expression from rREDs and aREDs with $k_{fold} > 0$ generally fell within the functional domain predicted by the mechanistic model, whereas devices with $k_{fold} < 0$ had more divergent behaviors.

Devising controls to coordinate the expression of multiple genes is an essential part of engineering synthetic biological systems (*2*). For instance, fine-tuned gene expression is critical for balancing fluxes in engineered metabolic pathways to prevent accumulation of toxic or bottleneck intermediates (*5*). As a proof-of-concept that RNA devices can generate predictable outputs in the context of high-titer production hosts, we designed rREDs to program the flux of *p*-AF, a chemical precursor of bioactive compounds (*24*) and industrial polymers (*25*) that is produced from a multicistronic biosynthetic operon (*26*). The transcript design method was used to search a library of R_{spc} hexamers to identify a sequence yielding efficient RBS and rbz folding across a set of devices ($\overline{d} = 0.54$, fig. S7). Component parts were subsequently assembled into devices expressing the three open reading frame (ORF) *papABC* operon (*27*) as part of a large, 12-gene engineered pathway in *Escherichia coli* (fig. S8). Although the *p*-AF flux generated by rRED15 was not significantly different from that of the reference device ($P = 0.05$, 12.1 ± 3.0 mg/l after 30 hours), the product titers from rRED16 (pred. = 53.7 ± 14.5, obs. = 44.3 ± 0.5 mg/l) and rRED17 (pred. = 65.1 ± 17.5, obs. = 51.3 ± 0.4 mg/l) were consistent with the design specifications.

Overall, for the rREDs and aREDs with $k_{fold} > 0$ there was excellent agreement between the predicted and measured outputs [relative root mean square deviation (rmsd) = 19%, Fig. 4]. Across the set of 25 rREDs and aREDs, one-way analysis of variance with k_{fold} showed that efficient transcript folding was an important determinant of programmable device function (F statistic = 10.8 on 3 and 21 df, $P = 6 \times 10^{-5}$). Supporting this view, there was much more divergence between predicted and observed γ_{rel} for the 12 devices constructed with $k_{fold} < 0$ (relative rmsd = 60%, table S7) than for the devices with $k_{fold} > 0$. Unexpectedly, there was also poor correspondence between the nascent transcript folds predicted with minimal free energy (*28*) RNA structure calculations and those generated with kinetic cotranscriptional folding simulations (table S5). Taken together, our results validate the mechanistic model, substantiate the role of transcript design and cotranscriptional folding simulations, and show that functional rREDs and aREDs can be assembled from component parts.

The successful development of a design-driven process to engineer programmable RNA devices with quantitatively predictable functions (fig. S1), demonstrated by the excellent fit between predicted and observed γ_{rel} ($r = 0.94$, $P = 1.3 \times 10^{-6}$), required coupling coarse-grained biochemical modeling with biophysical kinetic RNA folding simulations. This conceptual and experimental framework can be readily applied to study natural RNA activities, including ribozymes (*29*), riboswitches, and microRNAs (*6*, *12*). Programmable rREDs and aREDs have immediate utility as controllers for engineered metabolic pathways and genetic circuits (*10*) and, together with technologies for genome-scale modification (*30*), could be invaluable tools for implementing novel genetic programs. Our work establishes a foundation for developing computer-aided design platforms (*2*) to engineer complex RNA-based control systems that can process cellular information and program the expression of very large numbers of genes, enabling both increased understanding of fundamental biological processes and applications to meet demands for new therapies (*4*), renewable fuels, and chemicals (*5*).

References and Notes

1. C. Adami, *Bioessays* **24**, 1085 (2002).
2. J. D. Keasling, *Science* **330**, 1355 (2010).
3. R. M. Hazen, P. L. Griffin, J. M. Carothers, J. W. Szostak, *Proc. Natl. Acad. Sci. U.S.A.* **104** (suppl. 1), 8574 (2007).
4. A. S. Khalil, J. J. Collins, *Nat. Rev. Genet.* **11**, 367 (2010).
5. J. M. Carothers, J. A. Goler, J. D. Keasling, *Curr. Opin. Biotechnol.* **20**, 498 (2009).
6. J. Zhang, M. W. L. Lau, A. R. Ferré-D'Amaré, *Biochemistry* **49**, 9123 (2010).
7. H. Saito, T. Inoue, *Int. J. Biochem. Cell Biol.* **41**, 398 (2009).
8. C. C. Liu, A. P. Arkin, *Science* **330**, 1185 (2010).
9. X. Chen, A. D. Ellington, *PLOS Comput. Biol.* **5**, e1000620 (2009).
10. W. J. Holtz, J. D. Keasling, *Cell* **140**, 19 (2010).
11. Y. Benenson, *Curr. Opin. Biotechnol.* **20**, 471 (2009).
12. A. D. Garst, R. T. Batey, *Biochim. Biophys. Acta* **1789**, 584 (2009).
13. A. Deana, H. Celesnik, J. G. Belasco, *Nature* **451**, 355 (2008).
14. J. R. Kelly *et al.*, *J. Biol. Eng.* **3**, 4 (2009).
15. A. Saltelli *et al.*, *Global Sensitivity Analysis: The Primer* (Wiley, Chichester, UK, 2008).
16. M. N. Win, C. D. Smolke, *Proc. Natl. Acad. Sci. U.S.A.* **104**, 14283 (2007).
17. M. Martick, W. G. Scott, *Cell* **126**, 309 (2006).
18. K. H. Link *et al.*, *Biol. Chem.* **388**, 779 (2007).
19. J. M. Carothers, J. A. Goler, Y. Kapoor, L. Lara, J. D. Keasling, *Nucleic Acids Res.* **38**, 2736 (2010).
20. T. Pan, T. Sosnick, *Annu. Rev. Biophys. Biomol. Struct.* **35**, 161 (2006).
21. H. M. Salis, E. A. Mirsky, C. A. Voigt, *Nat. Biotechnol.* **27**, 946 (2009).
22. H. Isambert, *Methods* **49**, 189 (2009).
23. Materials and methods are available as supporting material on *Science* Online.
24. J. L. Duffy *et al.*, *Bioorg. Med. Chem. Lett.* **17**, 2879 (2007).
25. F. S. Sariaslani, *Annu. Rev. Microbiol.* **61**, 51 (2007).
26. B. F. Pfleger, D. J. Pitera, C. D. Smolke, J. D. Keasling, *Nat. Biotechnol.* **24**, 1027 (2006).
27. R. A. Mehl *et al.*, *J. Am. Chem. Soc.* **125**, 935 (2003).
28. C. Flamm, I. L. Hofacker, *Monatsh. Chem.* **139**, 447 (2008).
29. C.-H. T. Webb, N. J. Riccitelli, D. J. Ruminski, A. Lupták, *Science* **326**, 953 (2009).
30. H. H. Wang *et al.*, *Nature* **460**, 894 (2009).

Acknowledgments: Thanks to J. C. Anderson for the pLASC-lacpw plasmid; S. Lee and M. Hajimorad for technical advice; Y. Kapoor for technical assistance; and G. Bokinsky, W. Holtz, N. Hillson, and L. Katz for manuscript comments. D.J. and J.D.K. filed a provisional application for a U.S. Patent on the shikimate production module. Expression device sequences are presented in the supporting online material and in the Joint BioEnergy Institute (JBEI) Public Parts Registry at http://registry.jbei.org. Plasmids will be available from http://addgene.org upon publication. Supported by the Synthetic Biology Engineering Research Center (SynBERC) through NSF grant 0540879 and by JBEI through contract DE-AC02-05CH11231 between Lawrence Berkeley National Laboratory and the U.S. Department of Energy. J.M.C. was supported in part by a Jane Coffin Childs Postdoctoral Fellowship.

Supporting Online Material

www.sciencemag.org/cgi/content/full/334/6063/1716/DC1
Materials and Methods
SOM Text
Figs. S1 to S8
Tables S1 to S7
References (*31*–*51*)

4 August 2011; accepted 8 November 2011
10.1126/science.1212209